Classification and correction of the radar bright band with polarimetric radar

Will Hall[1], Miguel Angel Rico-Ramirez[1] and Stefan Krämer[2]

[1]*Department of Civil Engineering, University of Bristol, Bristol, BS81TR, UK*
[2]*Institute for Technical and Scientific Hydrology Ltd., Engelbosteler Damm 22, D-30167 Hanover, Germany*

(Dated: 16 July 2014)

Will Hall

1 Introduction

The quantitative estimation of precipitation with weather radars is error prone due to many different physical factors that affect the relation of radar measurements to surface observations (*Austin* 1986). The inhomogeneity of precipitation with height is one such problem due to the occurrence of bright bands (BB). The BB is an annular feature that occurs due to an enhancement of radar reflectivity returns from regions of melting snow (*Austin and Bemis* 1950). The horizontal reflectivity (Z_h) returns received by the radar are related to precipitation estimates through a power law equation. This can cause overestimations of rainfall intensity and accumulation at the surface by up to a factor of 5 (*Joss and Waldvogel* 1990) In order to reduce this overestimation the areal extent of the BB in radar scans must be classified and then corrected.

The current UK operational correction method is based on an algorithm by *Kitchen et al* (1994) which relies on forecasts of freezing level heights in addition to a fixed BB thickness of 700m to attain an estimate of the BB region. However, this does not allow for spatial and thickness irregularities in the BB which can occur due to atmospheric variability. The region of melting snow causing the BB effect can instead be classified based on multiple characteristics directly from dual-polarisation radar measurements (*Herzegh and Jameson* 1992; *Straka et al* 2000; *Liu and Chandrasekar* 2000). Research has shown that melting snow has a discernible signature when the linear depolarisation ration (LDR) and the horizontal reflectivity (Z_h) are compared (*Rico-Ramirez* 2005). A clear minimum in the cross-correlation coefficient (ρ_{hv}) and differential reflectivity (Z_{DR}) maximum were found to coincide with localised areas along the 1^{o}C isotherm (*Ryzhkov and Zrnic* 1998; *Matrosov et al* 2007; *Park et al* 2009) which further aids the classification of melting snow. These studies have used S- or X- band measurements whereas the current UK weather radar network uses C-band wavelengths which are more affected by attenuation than S-band but less so than X-band radars that are more frequently used for research purposes.

Correction of the BB can be performed through the use of an idealised vertical profile of reflectivity (VPR) (*Fabry and Zawadzki* 1995). *Kitchen et al.* (1994) found the application of different idealised VPRs at every pixel within the approximated BB area allowed for the potential to resolve small scale variations and that the greatest gains in accuracy were associated with the greatest precipitation rates. *Vignal et al* (2000) studied three methods of using VPRs to reduce precipitation estimation errors and found that the formation of mean profiles from volumetric scans offered large error reductions, while being more efficient and more robust than an identified, specific area profile method.

The aim is to create a more robust method that utilises measurements from an operational C-band polarimetric radar without needing to rely on numerical weather prediction outputs or extrapolation from surface observations. An algorithm will be presented that will automatically identify areas of enhanced reflectivity due to the melting layer in plan position indicator (PPI) scans. A model vertical profile of reflectivity (VPR) will be formed from the analysis of reflectivity scans and previous research (*Rico-Ramirez and Cluckie* 2008). Once the BB region has been identified, an algorithm based on the modelled VPR will be used to reduce rainfall overestimation by the radar.

2. Method and data

For this paper dual-polarisation data were utilised from an operational C-band radar located at Chenies, UK. All variables (Z_h, Z_{DR}, ρ_{hv}, and LDR) were measured at the first two elevations of the scanning strategy at 0.5° and 1.4° (hereto referred to as el0 and el1), while all except LDR were measured at the remaining three elevations 2°, 3°, and 4° (el2, el3 and el4 respectively). The lowest elevation suffered problems with ground clutter echoes and beam blockages while el1 and above are affected to a much lesser extent. Range bin lengths were 600m with a total range of 255km, with a radar beamwidth of 1°. Lower elevations also suffer more with beam spreading as the beam becomes wider with range causing an averaging of the VPR making it more difficult to distinguish the BB.

Initially all scans between 15th December 2013 and March 31st 2014 were analysed for possible BB events. Scans measuring LDR are produced every 10 minutes, with each event on average lasting 2 hours a total of over 200 scans were used, with ~2000 data points per scan. 10 events were judged to have a suitable BB signature, which was designated as an annular region of enhanced reflectivity. This region was then cross examined to check for areas of enhanced LDR (*Rico-Ramirez* 2005), minimums of ρ_{hv} (*Ryzhkov and Zrnic* 1998) and increased Z_{dr} which are associated with the freezing level (*Brandes and Ikeda* 2004), with a suitable example shown in Figure 1.

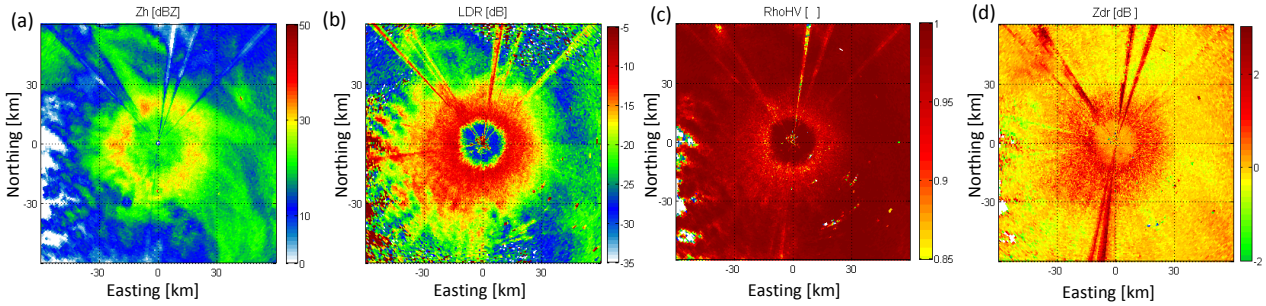

Figure 1. Example of a BB from 12/02/2014 measured as Z_h (a), LDR (b), ρ_{hv} (c), and Z_{DR} (d).

2.1 Membership functions

7 of the events were used as a database and 3 were used for validation purposes to assess the ability of the algorithm to classify and correct for the BB effect. Ground clutter and noise were removed before data processing using an algorithm demonstrated in *Rico-Ramirez and Cluckie* (2008). More than 100,000 data points from areas of snow, melting snow and rain were collected from the 7 events through the use of a program which allowed the user to highlight individual pixels and output the values into a separate file. The points were then fuzzified to form Membership Functions (MFs) based on the fuzzy logic system. Fuzzy logic works well as a classification system compared to Boolean logic type methods as it is faster, more robust and because hydrometeor measurement sets are not mutually exclusive (*Liu and Chandrasekar* 2000). The MFs are split into two hydrometeor groups as melting snow (BB) and as rain or snow (not BB). At all points the MFs are non-zero so that the product of all four MFs cannot be nullified.

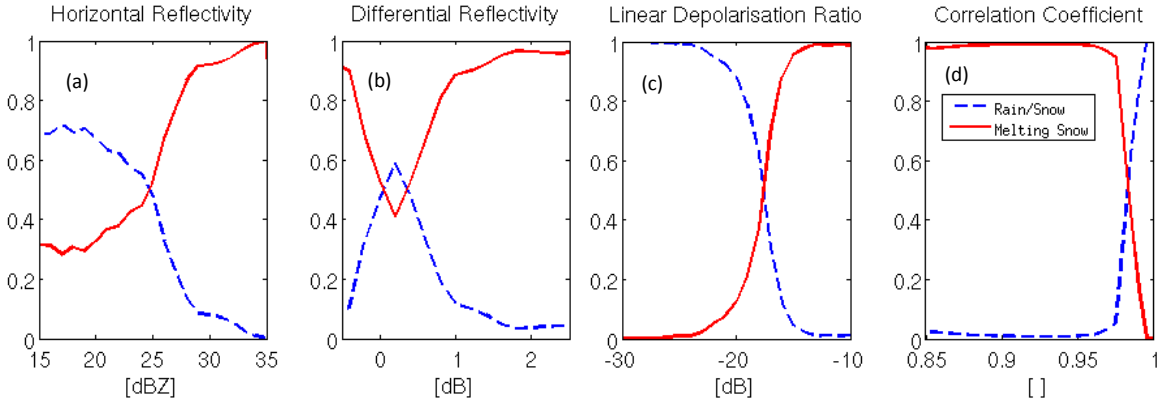

Figure 2. Membership functions for Z_h (a), Z_{DR} (b), LDR (c), and ρ_{hv} (d) to classify hydrometeors.

Figure 2(c) and (d) illustrate the importance of using LDR and ρ_{hv} as classifiers of melting hydrometeors due to the discernable signature and only a small area of overlapping region between the melting snow and rain/snow curve. Figure 2(b) shows the Z_{dr} maxima associated with the BB though there is a variation in the remaining section which reduces confidence in the classification ability. As the available data was restricted to winter months there was minimal high intensity rainfall (above 30dBZ) so the probability of pixels being BB increases to 1 beyond Zh values of 25dBZ. This however would make Zh unreliable as a sole identifier as it cannot distinguish between intense rainfall and BB overestimation, with its reliability worsening into summer months.

3. Results

3.1 Classifier

The result of hydrometeor classification for one of the three validation events is shown in Figure 3. Each pixel is analysed independently and classified as melting snow when the product of the corresponding MFs is greater than the rain/snow product. Along an azimuth the BB is determined to begin when 4 in 5 pixels are melting snow, and ends at the point where this average stops. A moving average filter that assigns lower weight to outliers is applied to the range of top and bottom pixels along the azimuths. The maximum value of horizontal reflectivity is then used as the BB peak, as it was found to offer a greater reduction of error during BB correction compared to setting the peak to be the mid-point. Figure 3 also illustrates the variation in BB thickness through each azimuth of the radar scan, with minimum of 310m to a maximum of 750m. The undefined region is due to erroneous data.

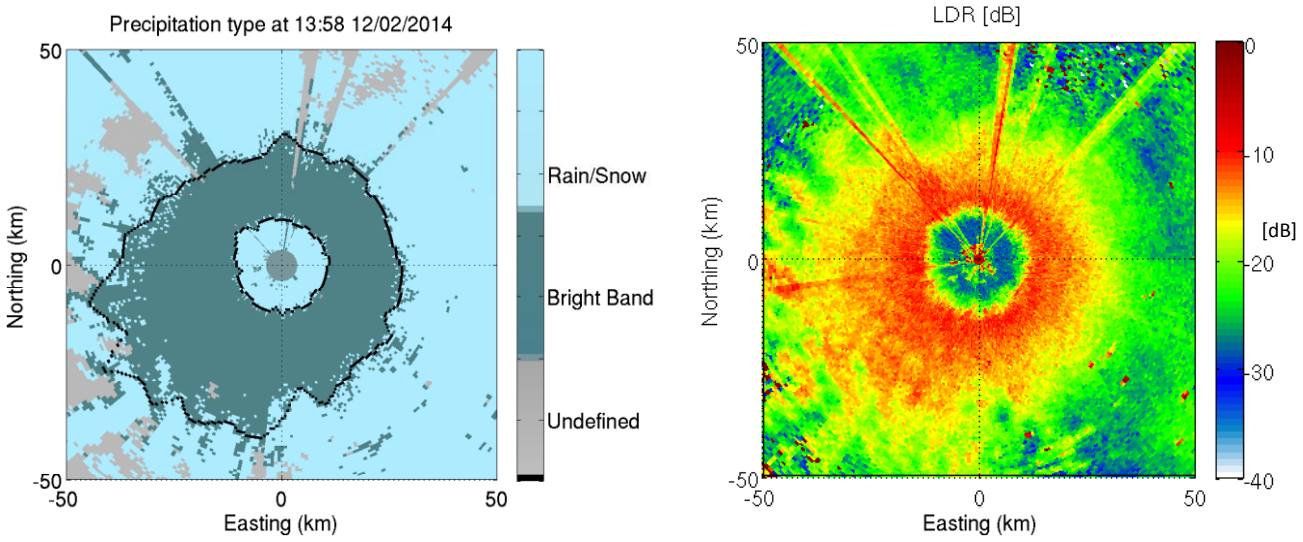

Figure 3. Classification of the BB area compared to an LDR scan at the same elevation and time for an event on the 12/02/2014. The black outline is the top and bottom of the BB region.

As scanning elevations above el1 do not measure LDR the effectiveness of the classification has also been tested using only ρ_{hv}, Z_h and Z_{dr} so that higher elevation scans can also be corrected. Figure 4 displays the Critical Success Index (CSI), an evaluation metric which incorporates false alarms (FAR), successful detections and missed events, with a value of 1 indicating a perfect classification. The difficulty of classification using only single polarisation data is shown

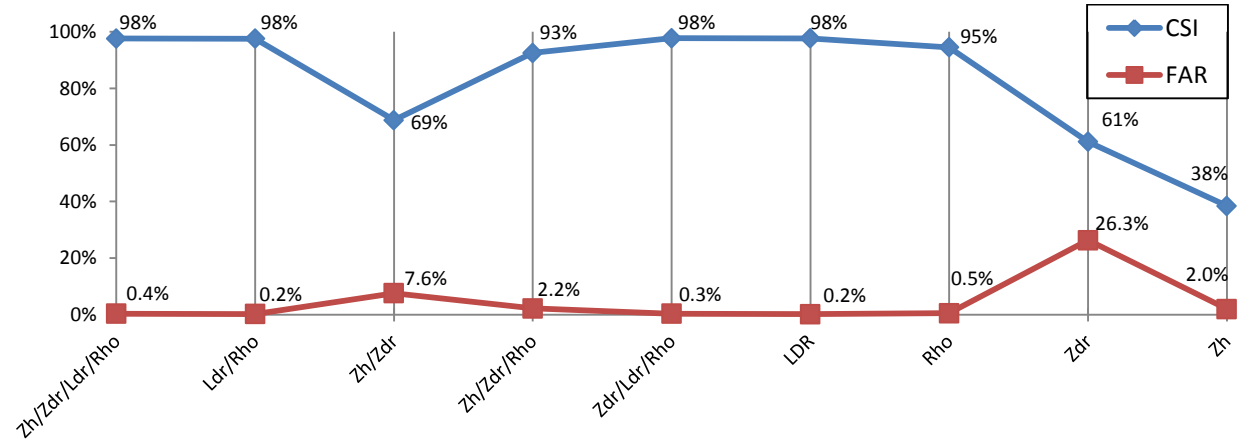

Figure 4. Critical Success Index (blue) and False Alarm Rate (red) for multiple variable combinations for classification tested with validation scans.

here with the low CSI for Zh, though added measurements including temperature profiles and freezing level forecasts could aid this if only single polarisation data were available. As mentioned in regards to figure 2 Zdr has difficulty classifying hydrometeors with near 0 values, and this is displayed by the high FAR. It was found that LDR greatly aids in the determination of the full extent of the BB, whereas ρ_{hv} was helpful for inner BB location but not for the outer section of the BB as values revert back toward 1, making the melting snow indistinguishable from snow or rain. Although LDR gives a good classification performance it suffers from propagation effects (*Chandrasekar et al* 1994*; Bringi and Chandrasekar* 2001), thus the use of other variables for classification can be beneficial. The overestimation of LDR increases with range and rain rate (*Herzegh and Jameson* 1992). This can be observed in figure 3 as a monotonic increase in LDR with range as the snow region has higher values than the central rain region.

3.2 Removal

In order to correct for the BB effect a modelled VPR is then assigned at each pixel between the classified BB top and bottom. The equations used to formulate the VPR are formed from extensive measurements of reflectivity values above, within, and below the BB from a radar experiment on the island of Jersey (*Rico-Ramirez and Cluckie* 2008),

- Zpeak = 11.74 + 0.91*Zrain (3.1)

- Zsnow = 2.23 + 0.69*Zrain (3.2)

where Zrain is a given value of reflectivity between 10 and 50 dBZ.

However, the modelled VPR cannot be directly compared to a VPR generated from radar reflectivity data as the radar will average values throughout the volume of the beam giving more weight toward the centre. This affect can be resolved using a method proposed by *Brown et al* (1991) and applied by *Kitchen* et al (1994) in which the VPR is averaged through the upper and lower limits of the radar beam, as shown by

$$Z_{ave} = \int_{\alpha}^{\beta} Z(\theta) f(\theta) d\theta \tag{3.3}$$

where Z(θ) is the modelled VPR value at the angle θ within the beam, α and β represent the bottom and top elevation of the radar beam and $f(\theta)d\theta$ is the fractional beam power at angle θ, as in

$$f(\theta)d\theta = \frac{P(\theta)d\theta}{\int_{\alpha}^{\beta} P(\theta)d\theta} \tag{3.4}$$

where P(θ) is the beam power profile, as shown in equation 5, in which 'k' is a constant that will vary according to the beamwidth.

$$P(\theta) = \left[\frac{\sin(k\theta)}{k\theta}\right]^4 \tag{3.5}$$

At every pixel the observed Z_h is then compared to the closest Z_{ave} and replaced by the corresponding Zrain value estimated below the BB and associated with the idealised VPR.

To judge the accuracy of the BB removal algorithm a lower elevation scan was used as a reference, as shown in Figure 5 and 6. At the lower elevation the BB will affect the beam at a range further from the radar and so the area directly beneath the upper beam will be unaffected. In Figure 5 the lower elevation scan (el0) can be seen to be heavily affected by beam blocking and ground clutter due to surrounding hills and buildings. However the general precipitation pattern can still be observed with the corrected el1 reflectivity scan being closer to el0 than the original el1. Figure 6

shows the correction using only Z_h, Z_{DR}, and ρ_{hv} for a higher elevation scan at el3. Here the lower elevation (el1) is less affected by beam blocking and clutter, but the BB is visible at the edges of the scan, though the corrected area here shows a good similarity.

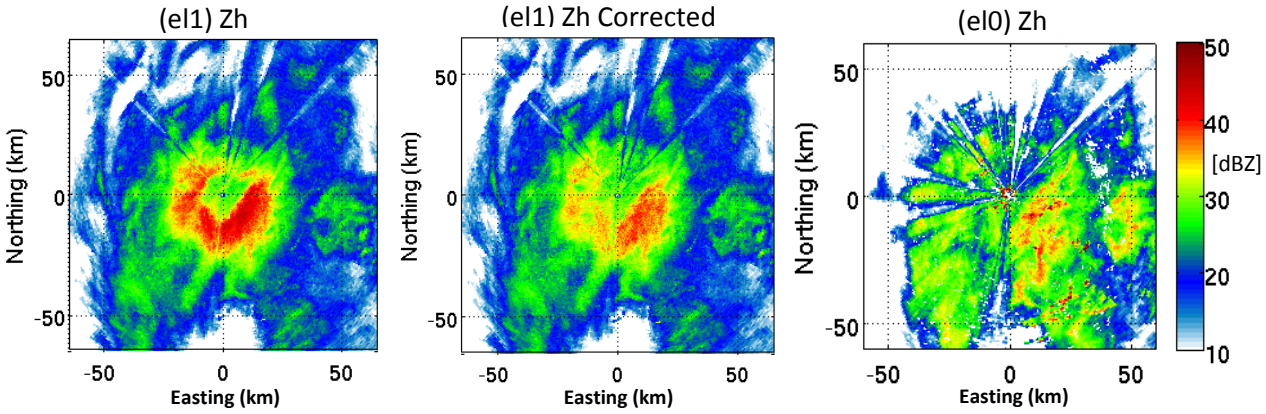

Figure 5. Correction of the BB at scan elevation el1 (1.4°) compared to the lower el0 (0.5°) for an event at 22:28 24/12/2013.

The Root Mean Square Error (RMSE) for the corrected el1 scans of Event 8 compared to el0 scans was 3.6 dBZ, with the uncorrected scans having an RMSE of 6.8 dBZ. For the 'weaker' event 10 the RMSE values were 3.8 dBZ and 6.0 dBZ for corrected and uncorrected el1 scans respectively. In total the reduction in RMSE was 2.8 dBZ with the correction applied for all scans throughout the three validation events.

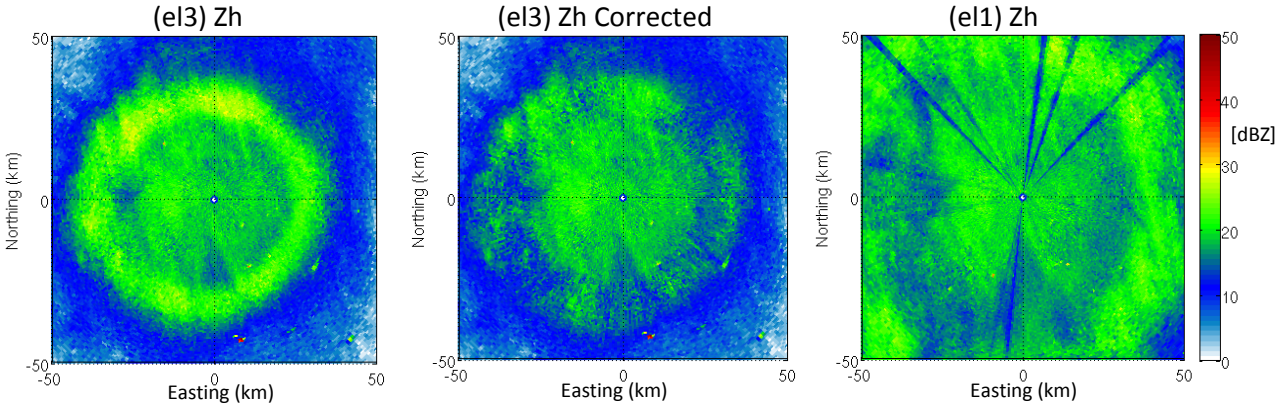

Figure 6. Correction of the BB at scan elevation el3 (3°) compared to the lower el1 (1.4°) for an event at 20:08 24/01/2014.

4. Conclusion

In this paper an algorithm was created that builds upon many previous methods to classify the BB and correct for the increased reflectivity measurements in this region. The current operational BB correction algorithm relies on forecasts and assumptions of constant BB thickness, whereas this can classify and correct using information only from operational C-band dual-polarised weather radar PPI scans. BB events were selected between December 2013 and March 2014 and used to create a database of rain, snow and melting snow pixels containing measurements of Z_h, Z_{DR}, LDR and ρ_{hv}. LDR was found to be the optimal classifier variable in the fuzzy logic system due to its strong signature in melting snow regions, though ρ_{hv} also had high CSI values as a lone classifier. When all classification variables were used and tested upon 3 validation events there was almost a factor of 2 reduction in RMSE compared to unaffected reflectivity region at lower elevations.

Acknowledgements

The authors would like to thank the UK Met Office for providing the polarimetric radar data through the British Atmospheric Data Centre to carry out this work.

References

Austin, PM, and AC Bemis, 1950: A quantitative study of the bright band in radar precipitation echoes. *J. Meteor.*, **7**,145–151.

----------, 1987: Relation between Measured Radar Reflectivity and Surface Rainfall. *Mon. Wea. Rev.*, **115**, 1053–1070.

Brandes EA, and K Ikeda, 2004: Freezing-level estimation with polarimetric radar. *J. Appl. Meteor***, 43:11**, 1541-1553.

Bringi, V. N., and V. Chandreskar, 2001: Polarimetric Doppler weather radar, principles and applications. Cambridge University Press, New York, 636pp.

Brown R, GP Sargent, and RM Blackall, 1991: Range and orographic corrections for use in real-time radar data analysis. *Hydrological applications of weather radar*, 219-228.

Chandrasekar, V., et al, 1994: Analysis and Interpretation of Dual-Polarized Radar Measurements at +45° and −45° Linear Polarization States. *J. Atmos. Oceanic Technol.*, **11**, 323–336.

Fabry F, and I Zawadzki, 1995: Long-Term Radar Observations of the Melting Layer of Precipitation and Their Interpretation. *J. Atmos. Sci.*, **52**, 838–851.

Herzegh PH, and AR Jameson, 1992: Observing precipitation through dual-polarisation radar measurements. *Bull. Amer. Meteor. Soc.* **73,** 1365-1374.

Joss J, and A Waldovogel, 1990: Precipitation measurement and hydrology. In *Radar in Meteorology: Battan Memorial and 40th Anniversary Radar Meteorology Conference*, Atlas D (ed). American Meteorological Society: Boston, MA; 577-606.

Kitchen M, R Brown, and AG Davies, 1994: Real time correction of weather radar data for the effects of bright band, range and orographic growth in widespread precipitation. *Q. J. R. Meteor. Soc.* **120**, 1231-1254.

Liu H, and V Chandrasekar, 2000: Classification of Hydrometeors Based on Polarimetric Radar Measurements: Development of Fuzzy Logic and Neuro-Fuzzy Systems, and In Situ Verification. *J. Atmos. Oceanic Technol.*, **17**, 140–164.

Matrosov SY, KA Clark, and DE Kingsmill, 2007: A Polarimetric Radar Approach to Identify Rain, Melting-Layer, and Snow Regions for Applying Corrections to Vertical Profiles of Reflectivity. *J. Appl. Meteor. Climatol.*, **46**, 154–166.

Park, HS, et al, 2009: The Hydrometeor Classification Algorithm for the Polarimetric WSR-88D: Description and Application to an MCS. *Wea. Forecasting*, **24**, 730–748.

Rico-Ramirez MA, ID Cluckie, and D Han, 2005: Correction of the bright band using dual-polarisation radar. *Atmos. Sci. Lett.*, **6**, 40–46.

---------- et al, 2007: A high-resolution radar experiment on the island of Jersey. *Met. Apps.* **14:2,** 117-129.

---------- and ID Cluckie, 2008; Classification of Ground Clutter and Anomalous Propagation Using Dual-Polarization Weather Radar, *IEEE TGARS*, **46:7,** 1892-1904.

Ryzhkov A and D Zrnic, 1998: Discrimination between Rain and Snow with a Polarimetric Radar. *J. Appl. Meteor.*, **37**, 1228–1240.

Straka J, D Zrnić, and A Ryzhkov, 2000: Bulk Hydrometeor Classification and Quantification Using Polarimetric Radar Data: Synthesis of Relations. *J. Appl. Meteor.*, **39**, 1341–1372.

Vignal B et al, 2000: Three methods to determine profiles of reflectivity from volumetric radar data to correct precipitation estimates. *J. Appl. Meteor.*, **39:10**, 1715-1726.